DTU Library

Modelling the Brillouin spectrum in Raman amplifier assisted Brillouin OTDR

Vandborg, Mads Holmark; Mariam Mathew, Neethu; Christensen, Jesper; Joy, Tomin; Allousch, M. Ali ; Marx, Benjamin; Jostmeier, Thorben; Grüner-Nielsen, Lars; Rishøj, Lars Søgaard; Rottwitt, Karsten

Published in:
Proceedings of 28th International Conference on Optical Fiber Sensors

Publication date:
2024

Document Version
Peer reviewed version

28th International Conference on Optical Fiber Sensors @ Optica Publishing Group 2023

Modelling the Brillouin spectrum in Raman amplifier assisted Brillouin OTDR

Mads Vandborg[1,*], Neethu Mathew[1], Jesper Christensen[2], Tomin Joy[3], M. Ali Allousch[3], Benjamin Marx[3], Thorben Jostmeier[3], Lars Grüner-Nielsen[1,4], Lars Rishøj[1], and Karsten Rottwitt[1]

[1] *Technical University of Denmark, Ørsteds Plads 343, 2800 Kgs. Lyngby, Denmark.*
[2] *Danish Fundamental Metrology, Kogle Allé 5, 2970 Hørsholm, Denmark.*
[3] *Luna Innovations Germany GmbH, Schanzenstrasse 39, Bldg. D9-D13, 51063 Cologne, Germany.*
[4] *Danish Optical Fiber Innovation, Åvindingen 22A, 2700 Brønshøj, Denmark.*

[*] *madshv@dtu.dk*

Abstract: We model and measure the Brillouin power spectrum of Brillouin OTDR assisted by Raman amplification. We show how Raman pump depletion leads to measurement errors due to spectral translation of the Brillouin spectrum.

1. Introduction

Brillouin optical time domain reflectometry (BOTDR) is a distributed fiber-optic sensing (DFOS) technique which is used to measure temperature and strain along an optical fiber. In BOTDR, a probe pulse is launched into an optical fiber, and the measurements are performed on the backscattered Stokes or anti-Stokes fields arising from spontaneous Brillouin scattering. A key advantage of BOTDR is that it enables long sensing ranges compared to other DFOS principles. Today, the maximum sensing range of BOTDR is limited by low SNR due to losses in the sensing fiber. To overcome these losses and increase the SNR, a solution is to amplify the probe signal during propagation using either Raman- of Erbium amplification. Recently, using combined Raman- and Erbium amplification, 250 km sensing range has been demonstrated for BOTDR [1] and 200 km has been shown for Brillouin optical time domain analysis (BOTDA) [2]. A system built entirely from Raman amplification might seem appealing since it requires no special fiber to be inserted along the sensing fiber. However, in recent studies [2,3] it has been shown that the pulse deformation due to depletion in the Raman amplification process can lead to a spectral shift in the spectrum of the backreflected Stokes or anti-Stokes fields, ultimately leading to errors in the measured temperature or strain.

In our previous work [3], we investigated numerically and experimentally the probe pulse deformation and the associated spectral shift of the spectrum due to depletion of the Raman pump. However, for BOTDR the measurements are performed utilizing the spectrum of the backward scattered Stokes or anti-Stokes field rather than the forward propagating probe field. In this paper, we therefore expand our analysis [3] to also numerically and experimentally investigate the spectrum of the backward scattered field. We present a model which we use to determine the spectrum of the backscattered Brillouin field, and we show by examples how the spectral shift evolves along a low-loss fiber for different Raman pump powers. Lastly, we compare the model to measurements, showing that the model explains well the observed spectral shift.

2. Modeling the Brillouin power spectrum of BOTDR

In this section, our goal is to find an expression for the power spectrum of the backscattered Brillouin field. Although the model will be validated against measurements of the anti-Stokes field, the same equations can be applied to model the Stokes field. For convenience, we denote the backscattered Brillouin field as the anti-Stokes field in the following analysis. For a pulsed probe field and a single CW Raman pump, we use the following propagation equations [4]

$$\frac{\partial A_p}{\partial z} + \frac{1}{v_p}\frac{\partial A_p}{\partial t} + \frac{1}{2}\alpha_p A_p = i\gamma_p\left(|A_p|^2 + (2-f_r)|A_{pr}|^2\right)A_p - \frac{1}{2}\frac{\omega_p}{\omega_{pr}} g_R |A_{pr}|^2 A_p, \tag{1a}$$

$$\frac{\partial A_{pr}}{\partial z} + \frac{1}{v_{pr}}\frac{\partial A_{pr}}{\partial t} + \frac{1}{2}\alpha_{pr} A_{pr} = i\gamma_{pr}\left(|A_{pr}|^2 + (2-f_r)|A_p|^2\right)A_{pr} + \frac{1}{2} g_R |A_p|^2 A_{pr}. \tag{1b}$$

where A are the amplitudes of the fields, with $|A|^2$ being the power in the fields, v is the group velocity, α is the linear fiber loss, γ is the nonlinear coefficient, $f_r = 0.18$, g_R is the Raman gain coefficient, and ω is the angular frequency. These equations include the nonlinear effects of stimulated Raman scattering, self-phase modulation (SPM) and cross-phase modulation (XPM). The equations are solved numerically using a split-step method for arbitrary input fields. The anti-Stokes field and the acoustic field are modelled as [5]

$$\frac{\partial A_s}{\partial z} - \frac{1}{v_s}\frac{\partial A_s}{\partial t} - \frac{1}{2}\alpha_s A_s = -\frac{1}{2}g_R|A_p|^2 A_s + i\omega_{pr} Q A_{pr} B^*, \tag{2a}$$

$$B(z,t) = \sqrt{\sigma}\int_{-\infty}^{t} e^{\frac{1}{2}\Gamma(t-t')} R(z,t')dt', \tag{2b}$$

where A_s is the amplitude of the anti-Stokes field, and B is the amplitude of the acoustic field. σ is the strength of the acoustic thermal noise, Γ is the acoustic decay constant and is related to the FWHM of the Brillouin spectrum (in Hz) as $\Gamma = 2\pi\cdot$FWHM. Q is a Brillouin coupling factor which is related to the Brillouin gain coefficient g_0 as $g_0 = 4\omega_{pr}\Omega|Q|^2 v_l/\Gamma$ where $\Omega = \omega_s - \omega_p$ is the resonance frequency of the acoustic mode, and v_l is the acoustic longitudinal velocity. $R(z,t)$ is a stochastic variable with zero mean and correlation $\langle R(z,t)R^*(z',t')\rangle = \delta(z-z')\delta(t-t')$. In Eq. (2a), the non-linear effects of stimulated Raman scattering and spontaneous Brillouin scattering are included.

To find the spectrum of a time-windowed part of the anti-Stokes field, we apply the short time Fourier transform (STFT) as

$$S(\omega, t_0) = \hat{F}_t\{h(t-t_0)A_s(z=0,t)\}, \tag{3}$$

where $\hat{F}_t\{\psi(t)\} = \int_{-\infty}^{\infty}\exp(+i\omega t)\psi(t)dt$ denotes the Fourier transform with respect to t. Here t_0 is the temporal center of the windowing function. In practice for our simulations, we employ a Hann window with a duration equal to the probe pulse duration. Following the approach presented in [6], we find that the stochastic equations (2) can be solved such that the ensemble average of the power spectrum is

$$\langle |S(\omega, t_0 = 2z_0/v_{pr})|^2\rangle = \kappa G(z_0)\int_0^L |\hat{F}_\tau\{A_{pr}(z_0,\tau)h(\tau + 2(z-z_0)/v_{pr})\}|^2 \overset{\omega}{*} g_B(\omega)dz. \tag{4}$$

In words, this equation shows that the power spectrum of the anti-Stokes field is a convolution in frequency domain between the Brillouin gain spectrum and the power spectrum of the windowed probe field. Here τ is a moving time frame, $\tau = t - z/v_{pr}$, and $\overset{\omega}{*}$ denotes the frequency domain convolution. We apply that $t_0 = 2z_0/v_{pr}$ is the relation between the distance to the scattering center z_0 and the time of flight t_0. $g_B(\omega)$ is the Brillouin gain spectrum and is given by $g_B(\omega) = g_0(\Gamma/2)^2/(\omega^2 + (\Gamma/2)^2)$ assuming that the optical fields excite only a single acoustic mode. $\kappa = \omega_b\sigma v_l/(\pi\Omega\Gamma)$ is a constant which determines the strength of the spontaneous Brillouin scattering. $G(z_0)$ is the net gain experienced by the backward travelling anti-Stokes field, and is a product of fiber loss and Raman gain. Since the pump field is not depleted by the weak anti-Stokes field, we assume the Raman pump to be non-depleted in this case, and hence the gain is calculated as $G(z_0) = \exp(-\alpha_{pr}z_0 + g_R|A_p(z=0)|^2 L_{eff})$ where $L_{eff} = (1-\exp(-\alpha_p z_0))/\alpha_p$. The advantage of having the analytical solution (4) is that we only need to know the evolution of the probe $A_{pr}(z,t)$ in order to predict the spectrum of the anti-Stokes field. This is less cumbersome than solving (2) numerically which is generally a complex task as the equations include stochastic variables.

3. Simulations of a Raman-assisted BOTDR

In this section, we theoretically investigate the anti-Stokes power spectrum arising from the co-propagation of a square probe pulse and a CW Raman pump. First, to demonstrate the physical effects during propagation, we simulate the evolution of the probe pulse and CW Raman pump using Eq. (1a) and Eq. (1b). In Figure 1a and 1d is shown the simulation of a probe square pulse of width 100 ns, peak power 50 mW at $\lambda_{pr} = 1550$ nm and a CW Raman pump with peak power 600 mW at $\lambda_p = 1480$ nm. We assume that the fiber is a Sumitomo ultra low loss (ULL) single-mode fiber and employ the fiber parameters as provided by the data sheet. From the simulation, we see the combined effect of temporal walk-off between the pump and probe and depletion of the pump (walk-off $v_p^{-1} - v_{pr}^{-1} = 1.27$ ns/km used for the simulations). Due to the walk-off, the trailing edge of the probe is Raman amplified by non-depleted pump power, whereas the leading edge is amplified by depleted pump power. This effect leads to a temporally dependent Raman gain which causes the probe pulse deformation [2,3]. In Figure 1b is shown the spectrum of the probe pulse. As also explained in [2], the asymmetric spectrum arises from SPM and XPM of the deformed pulse. Having calculated the probe spectrum, we make use of Eq. (4) to calculate the spectrum of the anti-Stokes field as shown in Figure 1e. We find that spectral shift of the probe pulse has transformed into spectral shift of the anti-Stokes spectrum, which ultimately transforms into a measurement error of the temperature or strain.

To expand the analysis, we have simulated the spectral shift of the anti-Stokes spectrum as a function of distance to the scattering center z for different pump powers as shown in Figure 1c. It is clear that increased Raman pump power leads to larger spectral shift. In 1f, we have plotted the associated power (normalized) of the anti-Stokes

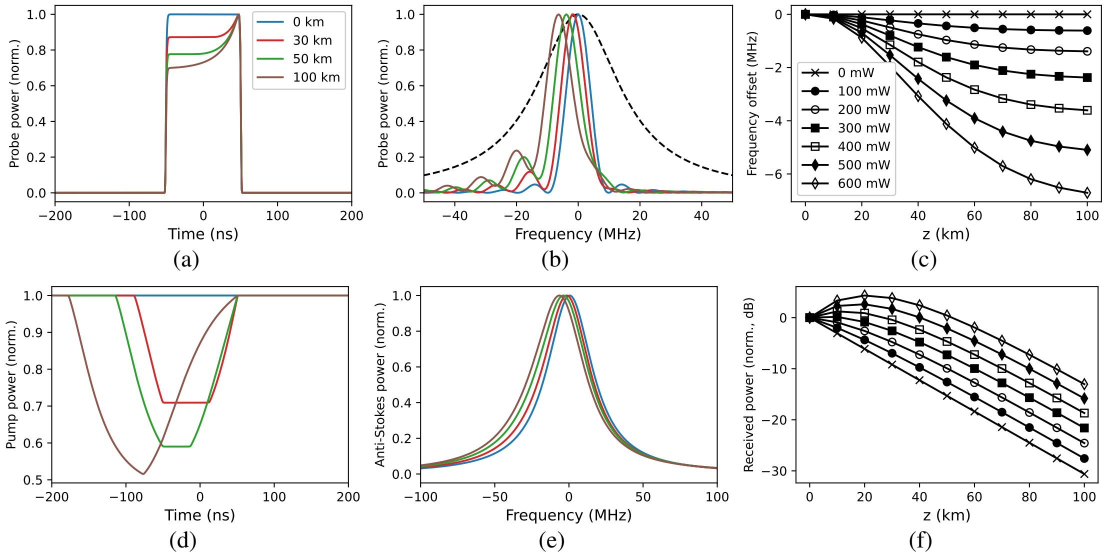

Fig. 1. (a) and (d) show the probe pulse and the Raman pump powers (normalized) in time domain for different positions in the fiber. The input probe pulse length is 100 ns, the input powers are 50 mW for the probe and 600 mW for the pump. (b) shows the spectra of the probe field, with the black-dashed line being the normalized Brillouin gain spectrum for comparison. (e) shows the anti-Stokes spectrum as calculated from Eq. (4). In (c) we have swept the pump power for some values in the range 0-600 mW (while keeping the probe pulse at 100 ns, 50 mW), and the figure shows the frequency shift of the peak of the anti-Stokes spectrum as a function of the location of the scattering center z. In (f) is shown the associated received Stokes power (normalized) as a function of z.

field at the receiver as a function of distance to the scattering center. As higher Raman pump power also leads to higher gain of the received anti-Stokes power, there is a clear trade-off between the gain of the received anti-Stokes field and the magnitude of the spectral shift. For silica fibers, a frequency shift Δf translates into a temperature shift as $\Delta f = C_T \Delta T$ with typically $C_T \approx 1.0°\text{C/MHz}$. It means that we find spectral shifts in the range 0-7 MHz or 0-7°C when converted to temperature.

4. Measurements

To verify the validity of the model presented in the former sections, we compare it to measurements performed in [7]. The experimental setup is shown in Figure 2. We use a commercial Brillouin OTDR interrogator (LIOS OTS4, LUNA Innovations) which launches a 100 ns, 1550 nm square pulse into Fiber 2 (Sumitomo Z-Plus 150, 20 km) and measures the backreflected anti-Stokes spectra. We use four laser diodes as Raman pumps which are combined into Fiber 1 (Sumitomo Z-Plus 150, 20 km). The Raman pumps and the probe are combined in Fiber 3 (Sumitomo ULL, 150 km). The Raman pump power is 0.6 W as measured after WDM2.

Figure 3 shows the modelled and measured anti-Stokes spectrum at $z \approx 69$ km for different probe powers with $z = 0$ being the position of the interrogator. For comparison, we have also shown the measured spectrum at $z \approx 23$ km, just after WDM2 (i.e. a spectrum which is not deformed). The measurements show a frequency shift of the anti-Stokes spectrum with the tendency that the magnitude of the frequency shift increases with pump power. The simulations show the same trend, but predicts a larger frequency shift than measured. Due to unknown (not measured) losses of the probe path in the experimental setup, the input probe power used for the simulations may be overestimated. This explains why the simulated frequency shift is too large.

5. Conclusion

We have modelled the backscattered Brillouin power spectrum of a Raman amplifier assisted BOTDR sensor, showing how the temporal depletion of the Raman pump leads to a spectral shift of both the probe field and its associated backscattered Brillouin field. The model shows a trade-off between the Raman gain and the induced frequency shift due to Raman pump depletion. When comparing to experiments, we find that the measured anti-Stokes Brillouin spectra show the same trend as the simulated spectra.

6. Acknowledgement

The authors acknowledge the support from Innovation Fund Denmark (grant no. 0224-00074B, GO-SENS), and the Danish Agency of Institutions and Educational Grants.

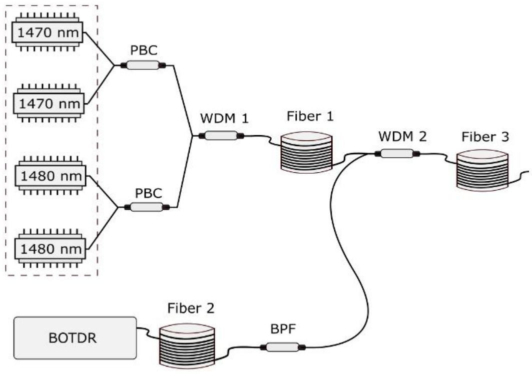

Fig. 2. Experimental setup. BPF: Band pass filter. WDM: Wavelength division multiplexer. PBC: Polarization beam combiner. Figure adapted from [1].

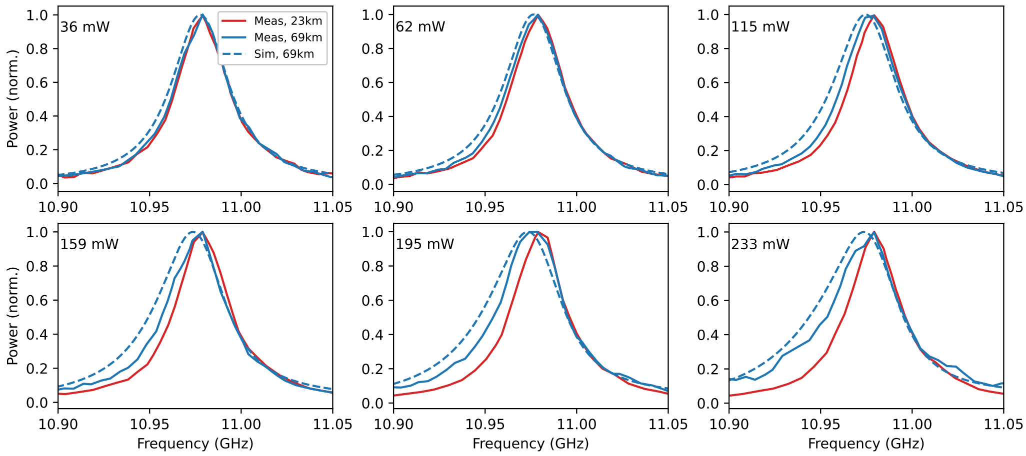

Fig. 3. The anti-Stokes spectrum at for different input probe powers in the range 36-233 mW. The solid blue line shows the measurement at $z = 69$ km, and the dashed blue line shows the simulation at $z = 69$ km as calculated from (4). The solid red line shows for comparison the measurement at $z = 23$ km. Measurement data is provided from [7].

References

1. T. Joy, T. Jostmeier, B. Marx, and W. Hill, "Increasing the Distance Range of Repeaterless Brillouin-OTDR to 250 km by Optical Amplification," in *27th International Conference on Optical Fiber Sensors*, p. W1.3, 2022.
2. Z. Yang, X. Sun, X. Hong, S. Jin, M. A. Soto, and J. Wu, "400 km-Loop BOTDA Enabled by Hybrid Amplification Based on Distributed Raman and Erbium-Doped Fibers," in *27th International Conference on Optical Fiber Sensors*, p. F2.1, 2022.
3. Z. Wang, M. H. Vandborg, T. Joy, N. M. Mathew, L. Grüner-Nielsen, L. S. Rishøj, J. B. Christensen, T. Jostmeier, B. Marx, W. Hill, and K. Rottwitt, "Mitigating probe pulse deformation in Raman amplification in OTDR fiber sensing systems," *Optics Express*, vol. 31, pp. 11457–11470, Mar. 2023.
4. G. P. Agrawal, *Nonlinear Fiber Optics*, ch. 8, pp. 302–205. Elsevier Inc., 6th ed., 2019.
5. O. A. Nieves, M. D. Arnold, M. J. Steel, M. K. Schmidt, and C. G. Poulton, "Noise and pulse dynamics in backward stimulated Brillouin scattering," *Optics Express*, vol. 29, no. 3, p. 3132, 2021.
6. K. Nishiguchi, C. H. Li, A. Guzik, and K. Kishida, "Synthetic spectrum approach for Brillouin optical time-domain reflectometry," *Sensors*, vol. 14, no. 3, pp. 4731–4754, 2014.
7. T. Joy, "Increasing the distance-range of repeater less brillouin otdr sensing by optical amplification," Master's thesis, Ruhr Universität Bochum and Luna Innovations Germany GmbH, 2022.